doi:10.1246/cl.2011.770

Published on the web June 25, 2011

Clustering and Octet Rule Violation Impact on Band Gap Bowing: Ab Initio Calculation of the Electronic Properties of $(GaAs)_{1-x}(Ge_2)_x$ Alloys

Hiroki Kawai, Giacomo Giorgi, and Koichi Yamashita*
Department of Chemical System Engineering, School of Engineering, The University of Tokyo, Tokyo 113-8656

(Received April 11, 2011; CL-110300; E-mail: giacomo@tcl.t.u-tokyo.ac.jp)

The asymmetry of $(GaAs)_{1-x}(Ge_2)_x$ band gap bowing, as a function of Ge concentration, is investigated by ab initio calculations. We show that the nature of the chemical bonds violating the octet rule in such alloys is affected by the local geometry: the switching of the cluster type between Ge to GaAs domain at Ge concentration of about 0.3 plays a fundamental role in the final asymmetry.

The increased attention that semiconductor alloys are currently attracting stems from their wide applicability in modern technological devices, in the field of electronics, in photonics, in light-emitting devices, and in photovoltaics. The most common class of semiconductor alloy is represented by the isovalent ones (i.e., IV/IV, (III–V)/(III–V), and (II–VI)/(II–VI)). On the other hand, the introduction of a low-valent and high-valent element into a III–V compound generates a nonisovalent alloy (i.e., (III–V)/IV and (III–V)/(II–VI)).[1] Their electronic and optical properties make this class of alloys extremely appealing. $(GaAs)_{1-x}(Ge_2)_x$, an $(A^{III}B^{V})_{1-x}(C_2^{IV})_x$ nonisovalent alloy, has direct band gaps (E_G) ranging between 0.5 and 1.4 eV, ideal for visible–IR light absorption, and lattice constants matching those of GaAs, representing the best candidate in relevant technologically oriented applications (i.e., for an extra junction to two junction $Ga_{0.52}In_{0.48}P$/GaAs solar cells[2]). The wide tunability of their direct gaps is realized by a large, negative, and asymmetric bowing as a function of Ge concentration (x), with a minimum value of $E_G \approx 0.5$ eV at $x \approx 0.3$.[3,4] This class of alloys has been investigated according to two structural parameters: long-range order (LRO), i.e., the measure of the order–disorder phase transition (GaAs, zincblend → Ge, diamond) and short-range order (SRO), i.e., nearest-neighbor atomic interaction. Previous work revealed how, at variance with LRO, SRO highly impacts the asymmetrization of the band gap bowing.[4,5] However, up to now, optimal structures representing the SRO behavior have not been fully clarified yet.

In the present paper, we aim at reproducing the asymmetric band gap behavior and confirming the role of SRO based on our previous approach,[6] combining density functional theory (DFT) and *GW* approximation.[7,8] In particular, DFT calculations were performed using the pseudopotential method with the projector-augmented wave (PAW)[9,10] potentials as implemented in the VASP code.[11] For both Ga and Ge d electrons were included in the semicore states. Cutoff energies of 288 and 581 eV were set as the expansion and augmentation charge for the plane wave basis. Geometric optimization results are at LDA level since in our previous work we showed that this approach better reproduces structural properties of GaAs and Ge.[6] The force convergence criterion was 0.01 eV Å^{-1}. The k-point sampling was $10 \times 10 \times 10$ for eight atom models, according to the Monkhorst–Pack (MP) scheme.[12] For the $n_x \times n_y \times n_z$ multiplied supercell models derived from the eight atom unit cell we used an $8/n_x \times 8/n_y \times 8/n_z$ k-points sampling scheme. Owing to the improved quality of calculated band gaps, we employed a GGA + GW_0 scheme,[13] which may be considered the most valuable *GW*-based approach,[8] since it gives band structures in very good agreement with experiments and, not trivially, it is less computationally demanding than full *GW* approximation. For the GGA calculations, we used the Perdew–Burke–Ernzerhof (PBE) exchange-correlation energy functional.[14] Cutoff energy for response function was 90 eV, and the number of frequency points for dielectric function was 48. The number of unoccupied bands was increased up to 200. The k-point sampling was $6 \times 6 \times 6$ Γ-centered for eight atom models. For the $n_x \times n_y \times n_z$ multiplied supercell models of the initial eight atom unit cell we used a Γ-centered $4/n_x \times 4/n_y \times 4/n_z$ k-point sampling.

Experimentally, it is reported that Ge regions start forming networks as the Ge concentration increased in the range $0 < x < 0.3$, and at $x \approx 0.3$ the networks connect each other, splitting the GaAs regions into smaller clusters.[15] Therefore, we based our study on models reproducing Ge-clusterized alloys at $0 < x < 0.3$ and GaAs-clusterized alloys at $0.3 < x < 1$. For investigating the relationship between the local geometry of the alloy (cluster shape and size in the host matrix) vs. the band gap opening, several representative extended alloy models with different local geometry and composition constituted by a number of atoms, ranging between 8 and 64, are analyzed. We here remark that the goal of our modelization is not to reproduce global minimum structures for each concentration. Since $(GaAs)_{1-x}(Ge_2)_x$ alloys are grown only at nonequilibrium condition,[3,4,16,17] i.e., metastable, we simply intend to confirm the experimental finding by analyzing several local minimum configurations.

The properties of all $(GaAs)_{1-x}(Ge_2)_x$ models are reported in Table 1. Here, the term "bad bond" means a chemical bond violating the octet rule[1] (i.e., Ga–Ge and As–Ge, see Figure 2) destabilizing the final systems. The domain size is the number of atoms in a finite cluster. Although experimental results report only the formation of GaAs clusters at $0.3 < x < 1$ alloys,[15] in order to compare and discuss local geometry effects we considered two models at $x = 0.375$: a Ge-clusterized (**IIIa**) and a GaAs-clusterized (**IIIb**) one. Table 1 shows that as the concentration of bad bonds increases the band gap response is different: it sharply decreases in Ge-clusterized models (**I**, **II**, and **IIIa**), while they only slightly reduces in GaAs-clusterized models (**IIIb**, **IV**, **V**, **VI**, and **VII**). **IIIb** has wider E_G than **IIIa**, revealing that at low Ge concentration, E_G continues decreasing as Ge concentration increases, as long as the alloy geometry is characterized by the presence of Ge clusters embedded in GaAs host. Differently, in the case that GaAs turns to clusterize in Ge network, the band gap stops decreasing. For the models with x

Table 1. Properties of $(GaAs)_{1-x}(Ge_2)_x$ alloy models

	x	Supercell size	Bad bond/%	Domain size		E_G/eV	
				GaAs	Ge	Direct	Indirect[a]
GaAs	0	1 × 1 × 1	0	∞	—	1.59	1.83
I	0.125	2 × 1 × 1	18.75	∞	2	1.23	0.92
II	0.25	2 × 1 × 1	31.25	∞	4	0.89	0.55
IIIa	0.375	2 × 1 × 1	43.75	∞	6	0.31	0.01
IIIb	0.375	2 × 1 × 2	75	5	∞	0.79	0.35
IV	0.50	2 × 1 × 2	62.5	4	∞	0.84	0.43
V	0.625	2 × 1 × 1	50	3	∞	0.72	0.59
VI	0.75	2 × 1 × 4	31.25	4	∞	0.76	0.71
VII	0.8125	2 × 1 × 2	25	3	∞	0.80	0.61
Ge	1	1 × 1 × 1	0	—	∞	0.94	0.92

[a]Owing to the symmetry dependence on the k-point sampling, only the direct band gap comparison on Γ is possible between these supercells. A full comparison with previous works where clusterization effects are not analyzed due to the reduced size of the considered cells (8 atoms)[6] cannot be performed.

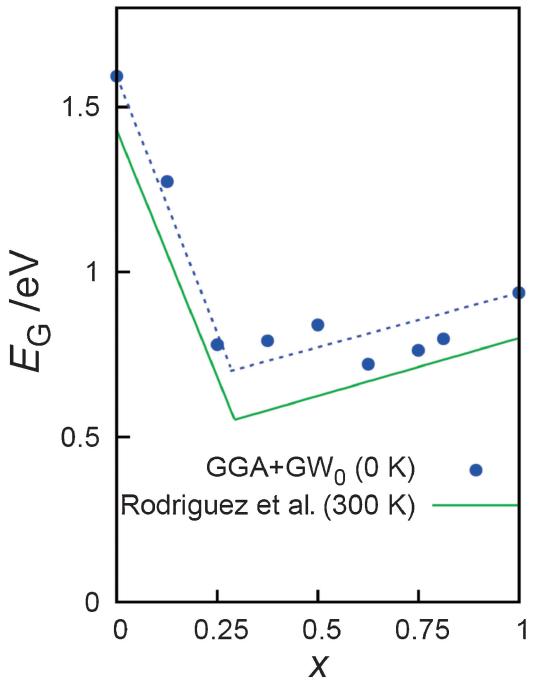

Figure 1. GGA + GW_0 calculated and experimental band gap behavior[4] vs. Ge concentration (x). Green solid line is fitted to experimental results by two line expressions. Blue points are the calculated values. The blue dotted line is fitted to blue points by two line expressions similar to the green solid line. At $x = 0.375$, the value of model **IIIb** is used.

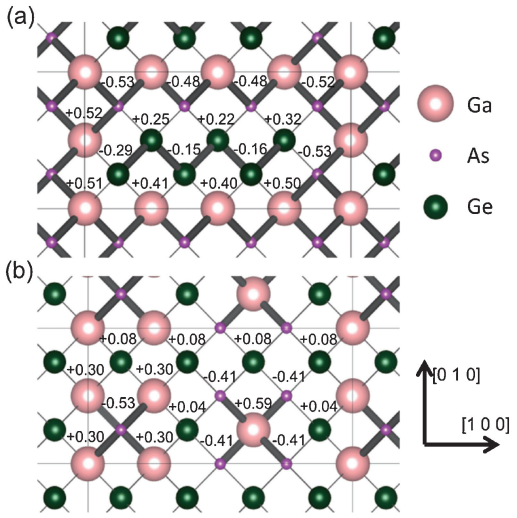

Figure 2. Structure and charge distribution for: top (a) **IIIa** and bottom (b) **IIIb** model. Bonds obeying the octet-rule are thick, while bad bonds are thin. The area surrounded by solid lines is the unit cell in the xy plane. Despite the in-plane visualization, bad bond counting is also along the [001] direction, i.e., perpendicular to the xy plane. According to Table 1, "domain size" corresponds to the number of Ge (a) and GaAs (b) atoms connected by thick bonds.

in the entire range between 0 and 1, further analysis is now in progress.[18] The relationship between the calculated direct gaps along all the range of x is reported in Figure 1. At $x = 0.375$, the value of model **IIIb** is used. The blue dotted line is fitted with the data at $0 \le x \le 0.30$ ($E(x) = 1.59 - 2.82x$) and $0.30 \le x \le 1$ ($E(x) = 0.61 + 0.33x$). The green solid line is the experimental one fitted with the optical absorption data for $(GaAs)_{1-x}(Ge_2)_x$ alloys at $T = 300$ K ($E(x) = 1.43 - 2.99x$: $0 \le x \le 0.30$, $E(x) = 0.45 + 0.35x$: $0.30 \le x \le 1$).[4] Although our calculated band gaps do not take into account thermal effects ($T = 0$ K), we observe that the slopes of our fittings closely overlap the experimental values obtained at 300 K, thus we are confident that our models are extremely suitable to reproduce the asymmetric band gap bowing of $(GaAs)_{1-x}(Ge_2)_x$ alloys, i.e., sharp decreasing at $0 < x < 0.3$ followed by a smooth increasing at $0.3 < x < 1$.

In $(GaAs)_{1-x}(Ge_2)_x$ alloys, the acceptors (Ga_{Ge}, Ge_{As}) and donors (As_{Ge}, Ge_{Ga}), when nearest-neighbors, are subjected to stabilizing self-compensation mechanisms[5] (Ga_{Ge}–As_{Ge} and Ge_{As}–Ge_{Ga}, respectively), while between atoms violating the octet rule (i.e., bad-bond pairs), this compensation does not occur due to the presence of residual local positive and/or negative charges. However, if such charges can be delocalized, the compensation can be effective even beyond nearest-neighbor

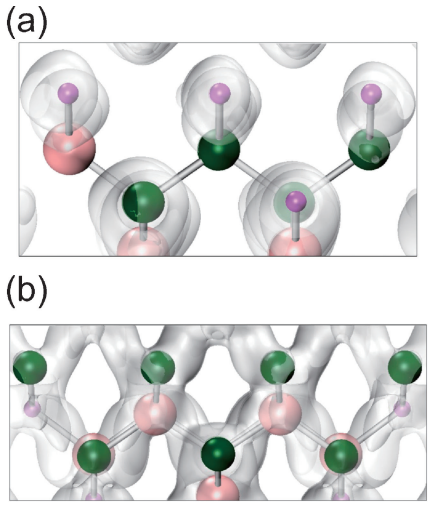

Figure 3. Isosurface of wave function on VBM of (a) model **IIIa** and (b) model **IIIb** [Online version, the colors of atoms are the same as Figure 2].

atomic sites. Thus, since the charge distribution on the bad bonds describes the nearest-neighbor atomic chemical environment, it represents a highly valuable analysis to estimate the SRO. In order to investigate the effect of the cluster type *switching* on bad bonds, we analyzed the charge distribution of **IIIa** and **IIIb** models according to Bader charge analysis.[19–21] Their structures and charges are shown in Figure 2. In "pure" GaAs, charge on Ga (As) atoms is +0.55e (−0.55e), with respect to the elemental species. In model **IIIa**, containing Ge clusters, the charges range between +0.40 and +0.52 for Ga, −0.53 and −0.48 for As, and between −0.29 and +0.32 for Ge. The charge reduction for Ga and As with respect to those of pure GaAs is easily explained in terms of electronegativity (χ); $\chi_{Ga} = 1.81$, $\chi_{Ge} = 2.01$, $\chi_{As} = 2.18$.[22] $\Delta\chi$ is smaller on bad bonds than on correct Ga–As bonds. Therefore, bad bonds locally induce destabilizing extracharges, being the destabilization counterbalanced by the possibility that charges have to delocalize. Charges on model **IIIb** are +0.30 on Ga, −0.41 on As, and +0.04/+0.08 on Ge, values extremely reduced if compared with those of **IIIa**. Such charge lowering is explained in terms of number of bad bonds that *single* Ga or As atom forms. In **IIIa**, each Ga and As atom forms 1 or 2 bad bonds. In **IIIb**, on the other hand, each Ga and As atom forms 3 bad bonds. The increase of bad bonds on single Ga and As atom causes partial delocalization of charges, as a consequence of the reduced $\Delta\chi$ between their constituting atoms.

Also the valence-band maximum (VBM) charge density at Γ is influenced by the alloy clusterization mechanism. Figure 3 reports the VBM charge density of **IIIa** and **IIIb**. In the case of **IIIa**, it is localized around the As and Ge, whose electronegativities are larger than Ga. This result is the direct consequence of the strong charge localization on their bad bonds. Thus, similarly to the valence band forward shift ascribed to the charge density localization (nonbonding), the sharp band gap decrease in the range $0 < x < 0.3$ must be also ascribed to the enhancement of the nonbonding character of the VBM. Differently, in **IIIb** the VBM is highly delocalized in the whole crystal. Here the strong bonding character of VBM stabilizes the system, causing the backward shift of VBM and also the smooth band gap opening at $0.3 < x < 1$, confirming that SRO effects play the main role in the asymmetric band gap bowing of this class of alloys.

In summary, we reproduced the asymmetric band gap bowing of $(GaAs)_{1-x}(Ge_2)_x$ alloys by modeling Ge-clusterized alloys at $0 < x < 0.3$ and GaAs-clusterized ones at $0.3 < x < 1$. In these latter models, an enhanced delocalization of local extracharges on the bad bonds is observed. The cluster switching, from Ge- to GaAs-type, at $x \approx 0.3$, increases the charge density delocalization on valence band maximum, explaining the asymmetrization of the band gap bowing of this class of alloys.

References and Notes

1 R. Osório, S. Froyen, A. Zunger, *Phys. Rev. B* **1991**, *43*, 14055.
2 A. G. Norman, J. M. Olson, J. F. Geisz, H. R. Moutinho, A. Mason, M. M. Al-Jassim, S. M. Vernon, *Appl. Phys. Lett.* **1999**, *74*, 1382.
3 S. A. Barnett, M. A. Ray, A. Lastras, B. Kramer, J. E. Greene, P. M. Raccah, L. L. Abels, *Electron. Lett.* **1982**, *18*, 891.
4 A. G. Rodriguez, H. Navarro-Contreras, M. A. Vidal, *Phys. Rev. B* **2001**, *63*, 115328.
5 L. C. Davis, H. Holloway, *Phys. Rev. B* **1987**, *35*, 2767.
6 G. Giorgi, M. van Schilfgaarde, A. Korkin, K. Yamashita, *Nanoscale Res. Lett.* **2010**, *5*, 469.
7 L. Hedin, *Phys. Rev.* **1965**, *139*, A796.
8 M. Shishkin, G. Kresse, *Phys. Rev. B* **2007**, *75*, 235102.
9 P. E. Blöchl, *Phys. Rev. B* **1994**, *50*, 17953.
10 G. Kresse, D. Joubert, *Phys. Rev. B* **1999**, *59*, 1758.
11 Vienna Ab-initio Simulation Package (VASP), Version 5.2.2, http://cms.mpi.univie.ac.at/vasp/, and references therein.
12 H. J. Monkhorst, J. D. Pack, *Phys. Rev. B* **1976**, *13*, 5188.
13 F. Fuchs, J. Furthmüller, F. Bechstedt, M. Shishkin, G. Kresse, *Phys. Rev. B* **2007**, *76*, 115109.
14 J. P. Perdew, K. Burke, M. Ernzerhof, *Phys. Rev. Lett.* **1996**, *77*, 3865.
15 T. C. McGlinn, M. V. Klein, L. T. Romano, J. E. Greene, *Phys. Rev. B* **1988**, *38*, 3362.
16 I. Banerjee, D. W. Chung, H. Kroemer, *Appl. Phys. Lett.* **1985**, *46*, 494.
17 Z. I. Alferov, M. Z. Zhingarev, S. G. Konnikov, I. I. Mokan, V. P. Ulin, V. E. Umanskii, B. S. Yavich, *Sov. Phys. Semicond.* **1982**, *16*, 532.
18 H. Kawai, G. Giorgi, K. Yamashita, to be submitted.
19 G. Henkelman, A. Arnaldsson, H. Jónsson, *Comput. Mater. Sci.* **2006**, *36*, 354.
20 E. Sanville, S. D. Kenny, R. Smith, G. Henkelman, *J. Comput. Chem.* **2007**, *28*, 899.
21 W. Tang, E. Sanville, G. Henkelman, *J. Phys.: Condens. Matter* **2009**, *21*, 084204.
22 See, e.g., WebElements: the periodic table on the web, http://www.webelements.com.

